THE JOURNAL OF BIOLOGICAL CHEMISTRY VOL. 284, NO. 35, pp. 23353–23363, August 28, 2009

Intersubunit Coupling in the Pore of BK Channels*[S]

Received for publication, March 13, 2009, and in revised form, June 25, 2009 Published, JBC Papers in Press, June 26, 2009, DOI 10.1074/jbc.M109.027789

Ying Wu[‡1], Yu Xiong[‡1], Sheng Wang[‡1], Hong Yi[§], Hui Li[‡], Na Pan[‡], Frank T. Horrigan[¶], Yingliang Wu[§2], and Jiuping Ding[‡3]

From the [‡]Key Laboratory of Molecular Biophysics, Huazhong University of Science and Technology, the Ministry of Education, Wuhan, Hubei 430074, China, the [§]State Key Laboratory of Virology, College of Life Sciences, Wuhan University, Wuhan, Hubei 430072, China, and [¶]Molecular Physiology and Biophysics, Baylor College of Medicine , Houston, Texas 77030

The structural basis underlying the gating of large conductance Ca^{2+}-activated K^+ (BK) channels remains elusive. We found that substitution of Leu-312 in the S6 transmembrane segment of mSlo1 BK channels with hydrophilic amino acids of smaller side-chain volume favored the open state. The sensitivities of channels to calcium and voltage were modified by some mutations and completely abolished by others. Interpretation of the results in terms of an allosteric model suggests that the calcium-insensitive mutants greatly destabilize the closed relative to the open conformation and may also disrupt the allosteric coupling between Ca^{2+} or voltage sensors and the gate. Some Phe-315 mutations also favor the open state, suggesting that Leu-312 and Phe-315 may interact in the closed state, forming a major energy barrier that the channel has to overcome to open. Homology modeling and molecular dynamic simulations further support that the side chain of Leu-312 can couple strongly with the aromatic ring of Phe-315 in neighboring subunits (L-F coupling) to maintain the channel closed. Additionally, single-channel recordings indicate that the calcium-insensitive mutants, whose kinetics can be approximately characterized by a two-state closed-open (C-O) model, exhibit nearly 100% open probability under physiological conditions without alterations in single-channel conductance. These findings provide a basis for understanding the structure and gating of the BK channel pore.

High conductance, "big" K^+ (BK)[4] channels encoded by the Slo1 gene are widely expressed in many tissues and respond to both membrane depolarization and submembrane Ca^{2+} concentration ($[Ca^{2+}]_i$) (1–4). Because BK channels have apparently evolved from voltage-dependent K^+ (K_V) channels, they share many features in common with K_V channels such as a similar K^+ selectivity filter and conserved ion conduction pore (5). On the other hand, detailed studies indicate that there are significant differences in the permeation and gating properties of K_V and BK channels. First, BK channels have the largest single-channel conductance among K^+ channels under similar recording conditions (6), partly because of two negatively charged rings at the entrance to the intracellular vestibule of BK channels that are absent from many K_V channels (7). Second, the mouth of the BK pore on the cytoplasmic side appears to be larger than other K^+ channels because the on-rates for channel block by quaternary ammonium (QA) ions are limited only by diffusion (8), whereas the on-rates for QA block of other K^+ channels are substantially slower. Additionally, it has been proposed that the pore-lining S6 segment of BK channels may not act as a permeation gate (8) as in Shaker K_V channels (9). Therefore, the BK channel may have an unusual pore, and understanding the structural basis of the above differences could provide important insight into the permeation and gating properties of K^+ channels.

Despite the differences between BK and K_V channels, it is likely that the opening and closing of their pores involve similar conformational changes. Flexing of the inner S6 helix at or near a conserved glycine residue is thought to open the pore, whereas straightening closes it (10, 11). The inner helix of BK channels is potentially more flexible than that of K_V channels because it contains a twin glycine motif (Gly-310–Gly-311). Differences in permeation property, pore geometry, and gating could potentially be accounted for by differences in S6 flexibility as well as the specific side-chain properties and interactions that occur between pore-lining residues. In this study we focused on Leu-312 and Phe-315 because we inferred from sequence analogy with KcsA channels (12) and our previous studies of BK channels (13, 14) that they are two of the five pore-lining residues (the others being Leu-309, Val-319, and Ile-323), and they are near the putative gating hinge. Our results indicate that substitutions of Leu-312 or Phe-315 have profound effects on BK channel gating, consistent with the notion that these residues interact between different subunits to hold the channel closed. The interaction of these residues may also be important for coordinating conformational changes in different subunits to ensure the efficient and cooperative long-range coupling between channel subunits, which is probably a general property of allosterically regulated proteins. Moreover, a surprising loss of Ca^{2+}- and voltage sensitivity that accompanies mutations of Leu-312 or Phe-315 raises the possibility that these residues play a broader role in allosteric communication between sensors and gates.

* This work was supported, in whole or in part, by National Institutes of Health Grant NS042901 (to F. T. H.). This work was also supported by National Science Foundation of China Grants 30770522, 30530140, and 30770519 and Program of Introducing Talents of Discipline to Universities Grant B08029.

[S] The on-line version of this article (available at http://www.jbc.org) contains supplemental Figs. 1–5.

[1] These authors contributed equally to this work.

[2] To whom correspondence may be addressed. Tel.: 86-27-6875-2831; Fax: 86-27-6875-2146; E-mail: ylwu@whu.edu.cn.

[3] To whom correspondence may be addressed. Tel.: 86-27-8779-2153; Fax: 86-27-8779-2024; E-mail: jpding@mail.hust.edu.cn.

[4] The abbreviations used are: BK, large conductance voltage- and Ca^{2+}-activated K^+; HEDTA, *N*-hydroxyethylenediaminetriacetic acid; WT, wild type; TEA, tetraethylammonium chloride; POPC, 1-palmitoyl-2-oleoyl-phosphatidyl-choline.

EXPERIMENTAL PROCEDURES

Site-directed Mutagenesis—Full-length cDNA for mSlo1 (accession number NP_034740) was subcloned into pcDNA3.1Zeo (+) (Invitrogen). Mutations were obtained by the QuikChange site-directed mutagenesis kit (Stratagene). To get the cRNA of mSlo1 and the mutants, cDNA of mSlo1 and mutants were subcloned into pXMX (a vector kindly provided by C. J. Lingle). All of the constructs were checked by sequencing. To prepare M7 GppGp-capped cRNA, the plasmids were linearized with Enzyme MluI and then *in vitro* transcribed by SP6 RNA polymerase (Roche Applied Science).

Cell Culture and Transfection—HEK293 cells were cultured in Dulbecco's modified Eagle's medium supplemented with 10% fetal bovine serum and grown in a 37 °C incubator with 5% CO_2. A day before transfection cells were transferred to 24-well plates. When 90% confluent, cells were transiently transected using Lipofectamine 2000 (Invitrogen). Electrophysiological experiments were performed 1–2 days after transfection.

Expression in Xenopus Oocytes—After DNA was linearized with MluI, SP6 RNA polymerase (Roche Applied Science) was used to synthesize cRNA for oocyte injection. 3–24 h after harvest, stage V-VI *Xenopus* oocytes were injected with 18–36 nl of RNA (10–20 ng/ml) using the Drummond Nanoject II (Drummond Scientific Co., Broomall, PA). After injection, oocytes were maintained in ND-96 solution at 18 °C. Currents were recorded 2–7 days after cRNA injection. ND-96 solution (pH 7.5) containing 96 mM NaCl, 2 mM KCl, 1.8 mM $CaCl_2$, 1 mM $MgCl_2$, and 10 mM H^+-HEPES was supplemented with 2.5 sodium pyruvate, 100 IU/ml penicillin, and 100 μg/ml streptomycin (incubation only).

Electrophysiology—All currents were recorded in excised patch configuration at room temperature (22–25 °C). Pipette resistance was typically 2–4 megaohms. Extracellular solution contained 160 mM $MeSO_3K$, 10 mM H^+-HEPES, and 2 mM $MgCl_2$, adjusted to pH 7.0 with $MeSO_3H$. High resistances seals were formed in a bath solution of ND-96. Intracellular solutions with different free Ca^{2+} were made by mixing 160 mM $MeSO_3K$ and 10 mM H^+-HEPES with $Ca(MeS)_2$ and 5 mM HEDTA (for 10 μM) or 5 mM EGTA (for 0 μM). Free Ca^{2+} was estimated by the EGTAETC program (E. McCleskey, Vollum Institute, Portland, OR) with the pH adjusted to 7.0. The tetraethylammonium chloride (TEA) or iberiotoxin (IbTX) solution was made by adding 20 mM TEA or 100 nM IbTX into the extracellular solution, and the lidocaine derivative QX-314 solution was made by adding 2 mM QX-314 into the intracellular solution. All chemicals were obtained from Sigma-Aldrich.

The Immunofluorescence Imaging of HEK293 Cells—HEK293 cells were transiently transfected with c-Myc-tagged channels and plated on poly-D-lysine-coated chambers. The next day cells were fixed with 2% paraformaldehyde in phosphate-buffered saline for 5 min. For cell permeabilization, 0.2% Triton X-100 was added for 5 min. After blocking for 1 h with 5% goat serum, cells were incubated with a monoclonal anti-human c-Myc antibody (1:150) for 5 h, washed, and incubated with fluorescein isothiocyanate-conjugated anti-mouse IgG (H+L) (1:100) for 1 h. All the experiments were performed at room temperature (about 25 °C). We took advantage of the high numeric aperture objective (APO·100 OHR, NA = 1.65, Olympus) to take high-resolution fluorescence images of the transfected HEK293 cells. Excitation light from a fiber optical coupled monochromator (Polychrome IV; TILL Photonics GmbH, Germany) was passed through a shutter that opened only during camera exposure. The wavelength selection and switch were controlled by the image acquisition software (TILL vision 4.0; Till Photonics GmbH). Images were acquired with a cooled CCD (PCO SensiCam) with a pixel size of 0.067 μm at the specimen plane. Images were viewed, processed, and analyzed in TILL Vision (TILL Photonics), Adobe Photoshop (Adobe Systems), and IMAGE J (National Institutes of Health). The exposure time was 2000 ms, and the percentage of fluorescent intensity was calculated from the target cells.

Data Analysis—Data were analyzed with IGOR (Wavemetrics, Lake Oswego, OR), Clampfit (Axon Instruments, Foster city, CA), SigmaPlot (SPSS Science, Chicago, IL), and QuB software package (State University of New York at Buffalo). Unless stated otherwise, all data are plotted as the means ± S.D. ($n \geq 4$), although *error bars* were often smaller than the symbol size; the V_{50}-$[Ca^{2+}]_i$ curves of mSlo1 and its mutants were analyzed by a two-way analysis of variance test (factor A, $[Ca^{2+}]_i$; factor B, mutation), and differences in their values were considered significant at a probability of ≤ 0.05. The single channels were recorded with an EPC-9 patch clamp amplifier and PULSE and PULSEFIT software (HEKA Elektronic, Lambrecht/Pfalz, Germany), sampled at 20 kHz, and filtered to 10 kHz. Macropatch currents were filtered at 3 kHz. Single-channel currents were analyzed and simulated with QuB software from SUNY at Buffalo. Idealization was done using the segmentation k-means algorithm after digital low-pass filtering to 10 kHz. Kinetic modeling of the idealized intervals was done using the maximum interval likelihood method.

The G-V curves for activation were generated from steady-state or tail currents, converted to conductance, and then fitted by the single Boltzmann function with the form

$$G/G_{max} = (1 + \exp((V - V_{50})/\kappa))^{-1} \quad \text{(Eq. 1)}$$

where V_{50} is the voltage at which the conductance (G) is half the maximum conductance (G_{max}), and κ is a factor affecting the steepness of activation.

The open probability of the steady-state BK current described by a 50-state allosteric model (Cox and Aldrich (18)) is given by the function

$$P_{open} = \frac{1}{1 + \left(\frac{(1 + [Ca^{2+}]/K_C)}{(1 + [Ca^{2+}]/K_O)}\right)^4 \times \left[\frac{(1 + e^{ZF(V - Vh_C)/RT})}{(1 + e^{ZF(V - Vh_O)/RT})}\right]^4 \times L(0) \times e^{\frac{-QFV}{RT}}} \quad \text{(Eq. 2)}$$

where $[Ca^{2+}]$ is the cytosolic Ca^{2+} concentration, K_C(K_O) is the dissociation constant of Ca^{2+} from the binding sites when the channel is closed (open), Z represents the equivalent gating charge associated with each voltage sensor's movement, Vh_C (Vh_O) represents the voltage at which a single voltage sensor is half the time active when the channel is closed (open), $L(0)$ represents the open-to-closed equilibrium constant when no voltage sensors are active and no Ca^{2+} binding sites are occu-

pied, Q represents the equivalent gating charge associated with this equilibrium, R is the gas constant, T is temperature, and F is Faraday's constant.

Protein Modeling and Molecular Dynamics Simulation—All the MD simulations of membrane proteins in this study were carried out with the phospholipid bilayer solvated by water to provide the optimum environment. All of the wild type mSlo1, L312F, and L312I mutation models (only S5-P-S6) were constructed by homology modeling using modeler 9v2. The template was the crystal structure KCSA (PDB code 1BL8). A pre-equilibrated 1-palmitoyl-2-oleoyl-phosphatidyl-choline (POPC) bilayer with 274 lipid molecules was obtained from VMD 1.8.6, and the protein was embedded in the pre-equilibrated POPC lipid bilayer with the main axis along the z direction of bilayer POPC membrane. A cylindrical hole was made in the center of the bilayer by removing lipids whose P atoms fell within 2.0 Å of the above models. These whole systems were solvated (TIP3) and ionized in the presence of 160 mM KCl on both sides of the POPC membrane. A short MD simulation with a radially acting repulsive force was used to drive any remaining atoms out of the cylinder and into the bilayer. An initial minimization process was conducted for a 1-ns period to remove the bad contacts of intramolecular residues and between models and POPC molecules. The final production of MD simulations was performed for 2 ns to produce final equilibrated conformation. All of the simulations were using the Amber 8 suites (15) on a 66-CPU Dawning TC4000L cluster (Dawning Information Industry Co., Ltd., Beijing, China). The ff99 force field (Parm99) was applied throughout the energy minimization and MD simulations.

RESULTS

The pore domains of many K^+ channels share identical amino acid sequences in the selectivity filter and a glycine residue in the inner helix (supplemental Fig. 1*A*) that may act as a gating hinge (10). Although this homology suggests that key structural elements of the permeation pathway are conserved, the pores of different K^+ channels also contain unique features that may underlie differences in permeation and gating properties. For example, the inner helix of Shaker-family channels (*e.g.* Kv1.2) bends at a PVP sequence (supplemental Fig. 1*A*) that is lacking in other K^+ channels, resulting in a differences in pore geometry and interaction among pore-lining residues (11, 16). Likewise, the BK channel contains, adjacent to the putative glycine hinge, an additional glycine (supplemental Fig. 1*A*) that is implicated in gating (10) and could potentially account for unique properties of the BK channel pore by conferring increased flexibility to the inner helix.

To help determine whether the BK channel pore structure deviates from that of other K^+ channels near the putative gating hinge, we compared the arrangement of pore-lining residues in three K^+ channels of known structure (supplemental Fig. 1, *B–D*). The crystal structures of KcsA, MthK, and $K_V1.2$ suggest that two consecutive hydrophobic pore-lining residues after the putative glycine hinge, equivalent to Leu-312 and Phe-315 in the BK channel, may interact between adjacent subunits (Ile-100/Phe-103 in KcsA; Ile-84/Phe-87 in MthK; Val-399/Ile-402 in $K_V1.2$) because they come within an average contact distance of 4 Å (supplemental Fig. 1, *B–D*). The location of these residues, intracellular to the gating hinge and in different subunits, suggests their relative position and interaction could change during channel gating. For example, they may interact more strongly in the closed than the open conformation, as suggested by their closer apposition in KcsA (closed) *versus* MthK or Kv1.2 (open). Consistent with this possibility in BK channels, we found previously that that substitution of leucine at position 312 with alanine (L312A) markedly increases open probability, unlike mutation of an adjacent presumptive pore-lining residue (L309A) (14), suggesting Leu-312 could be involved in a state-dependent interaction. In the present study we examined in more detail the roles of Leu-312 and its potential interaction partner Phe-315 in BK channel gating.

Leu-312 Mutations Enhance BK Channel Activation—Using site-directed mutagenesis, we probed the role of Leu-312 in BK channel gating. Representative current traces and their corresponding conductance-voltage (G-V) curves are plotted for wild type (WT) mSlo1 (Fig. 1*A*) and seven mutants (Fig. 1, *B–H*) at different $[Ca]_i$, from 0 to 2 mM. With the exception of a hydrophobic substitution (L312F, Fig. 1*B*) that had a slight effect on steady-state activation compared with the WT, every mutation tested shifted G-V relations to more negative voltages in the presence or absence of Ca^{2+}, in some cases by hundreds of millivolts (Fig. 1, *C–H*). This marked enhancement of channel activation tended to increase as the hydrophobicity and/or size of the side chain at position 312 was reduced, consistent with the possibility that Leu-312 is involved in a hydrophobic interaction that normally stabilizes the closed conformation.

Leu-312 Mutations Alter Ca^{2+} and Voltage Sensitivity—Mutations of Leu-312 not only facilitated channel opening but also differentially altered the Ca^{2+} and voltage sensitivity of steady-state activation. Shifts in the G-V to more negative voltages were generally accompanied by a reduction in G-V slope (Fig. 1); that is, a decrease in apparent voltage sensitivity. Some mutants in which G-Vs were shifted relative to the WT in 0 Ca^{2+} exhibited large additional shifts in response to Ca^{2+}, like the WT (*L312I* and *L312W*, Fig. 1, *C–D*). Surprisingly, however, mutations that produced the largest G-V shifts in 0 Ca^{2+} (L312C, L312V, L312S, L312Q) also abolished Ca^{2+} sensitivity such that G-Vs in different Ca^{2+} concentrations superimpose (Fig. 1, *E–H*).

To quantify the effects of Leu-312 mutation, the half-activation voltage (V_{50}) and the change in V_{50} relative to 0 Ca^{2+} ($\Delta V_{50} = V_{50}([Ca^{2+}]) - V_{50}(0\ Ca^{2+})$) for each mutant were plotted as functions of Ca^{2+} concentration (Fig. 2). L312I and L312W both shifted V_{50} by approximately −100 mV relative to the WT in 0 Ca^{2+} (Fig. 2*A*) and exhibited Ca^{2+}-dependent changes in V_{50} over a similar concentration range as the WT (Fig. 2*B*). However, the maximal ΔV_{50} values for these two mutants were different and suggest that L312I reduces Ca^{2+}-sensitivity. In the case of L312W, the magnitude of ΔV_{50} was clearly greater than the WT at all $[Ca^{2+}]$, albeit difficult to quantify accurately for Ca^{2+} concentrations ≥10 μM where V_{50} was shifted below the experimental voltage range (Fig. 1*D*). This enhanced response to Ca^{2+} probably reflects the reduced G-V slope of L312W. A reciprocal relationship between apparent charge (G-V slope) and ΔV_{50} is expected based on the energetic additivity of Ca^{2+}- and voltage-dependent BK channel activation

(17). Therefore, an increased ΔV_{50} of L312W does not necessarily indicate a change in the energetic efficacy of Ca^{2+} binding on channel opening. By contrast, L312I exhibited a significantly smaller ΔV_{50} than the WT ($p < 0.000003$) despite a reduced G-V slope, implying a decrease in the efficacy of Ca^{2+}. Similarly, the lack of Ca^{2+} sensitivity exhibited by L312C, L312V, L312S, and L312Q (Fig. 2*B*) is remarkable because the G-Vs of these mutants are approximately half as steep as the WT ($\kappa > 51$ mV/e-fold), which should accentuate any residual effect of Ca^{2+} on V_{50} in these mutants.

Effects of the Leu-312 Mutations on Activation and Deactivation Kinetics—Currents evoked with some of the less hydrophobic substitutions (L312C, L312V, L312S, L312Q) exhibited nearly instantaneous activation and deactivation (Fig. 1, *E–H*), likely reflecting that channels are open, even at the −180 mV pre-pulse voltage. To identify the property of these leak-like currents, two K^+ channel blockers, QX-314 and TEA, were used for L312S and L312V (supplemental Fig. 2). Application of intracellular 2 mM QX-314 to inside-out patches blocked these currents almost completely in a reversible manner (supplemental Fig. 2*A*). Similarly, extracellular 20 mM TEA reversibly inhibited L312S and L312V currents in outside-out patches to a similar extent as the WT (supplemental Fig. 2*B*). Additionally, a selective inhibitor of BK channels, 100 nM iberiotoxin, was extracellularly applied to L312Q and blocked the currents almost completely (supplemental Fig. 3). Thus, we conclude that currents were indeed carried by mutant BK channels that are open at negative voltages.

The time constants of activation (τ_a) and deactivation (τ_d) for Ca^{2+}-insensitive mutants L312C, L312V, L312S, and L312Q were much faster than the bandwidth of our recordings (100 kHz) and could not be determined (Fig. 1; supplemental Fig. 2). However, we were able to

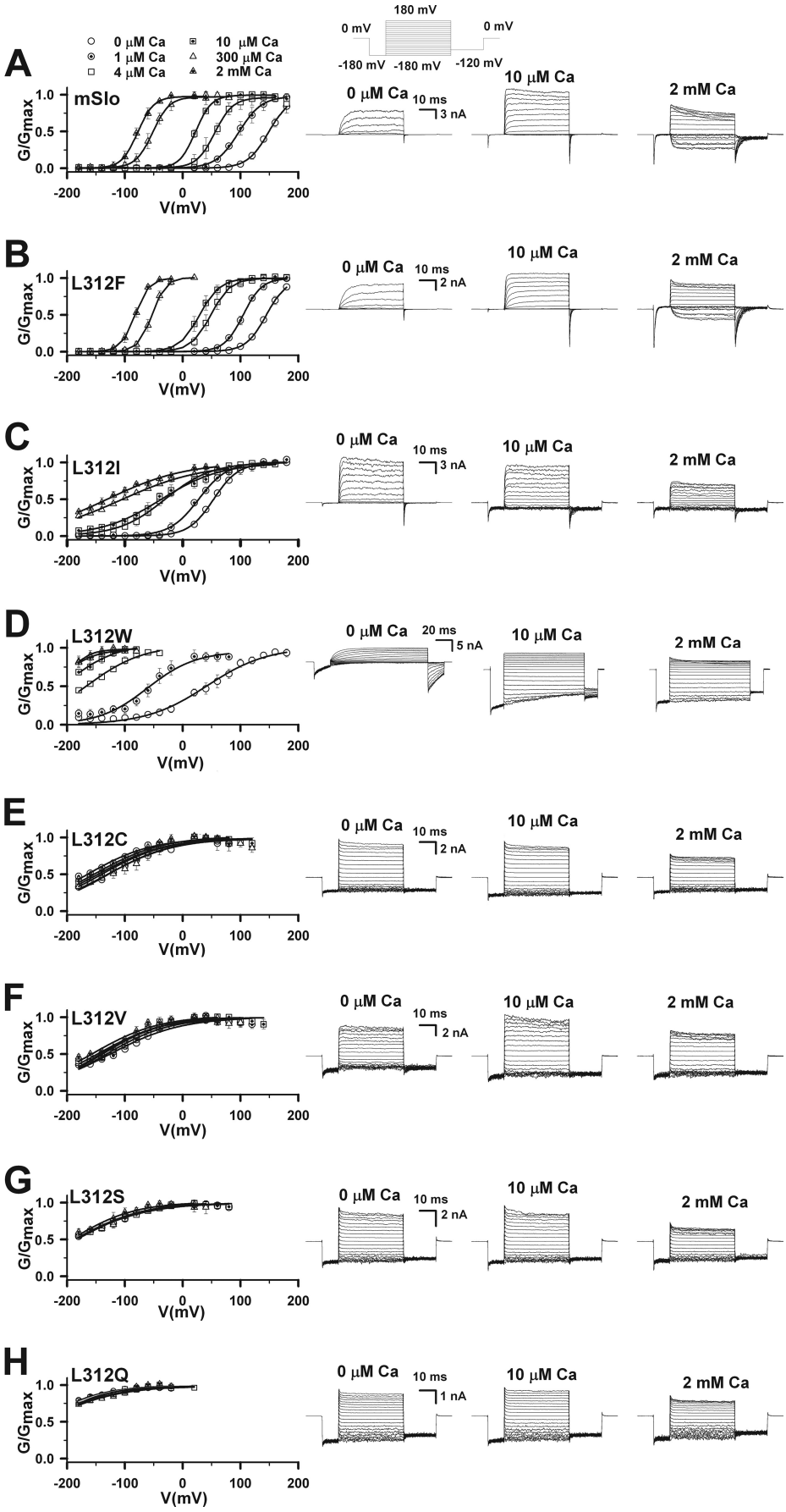

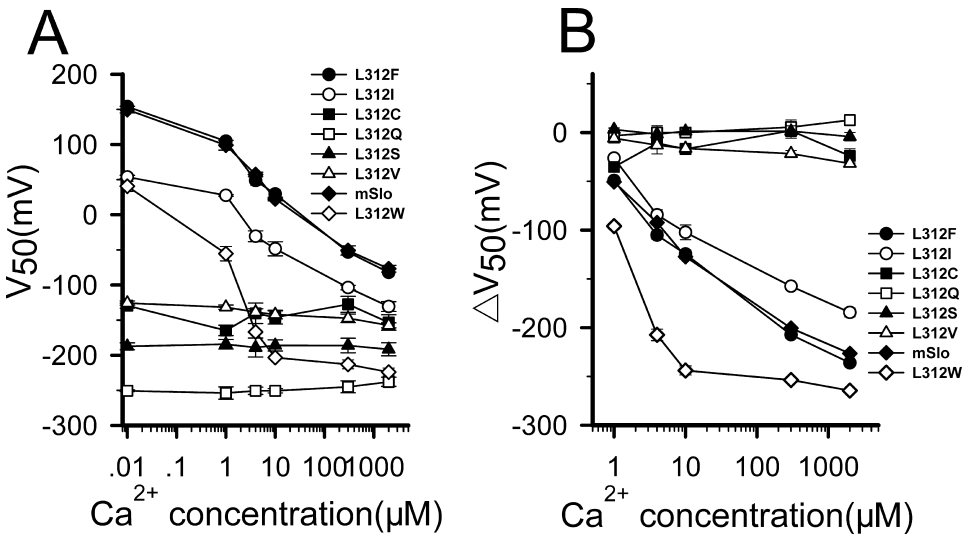

FIGURE 2. **The Ca^{2+} dependence of Leu-312 mutants.** The values of V_{50} (*A*) and ΔV_{50} (in *B*) for each Leu-312 mutant are plotted as a function of $[Ca^{2+}]_i$. *Error bars* indicate S.D. ($n \geq 4$). Statistical significance of the datasets (*A*) as a whole was determined by a two-way analysis of variance test with $p < 0.001$ for both factor $[Ca^{2+}]_i$ and mutation.

reliably measure these time constants for the Ca^{2+}-sensitive mutants. τ_a and τ_d are plotted as a function of voltage and Ca^{2+} concentrations for WT, L312F, and L312I in Fig. 3. L312F and L312I exhibit voltage dependence similar to that of WT (Fig. 3). However, the time constants of L312I were far less calcium-dependent than the WT, supporting the conclusion that L312I reduces Ca^{2+} sensitivity. In the case of L312F, it is notable that both activation and deactivation were slower than that of the WT at all $[Ca^{2+}]$. Thus, L312F does have effects on opening and closing kinetics despite a failure to alter steady-state activation (Figs. 1, *A* and *B*, and 2*A*).

The Mechanism of Leu-312 Mutation Action—Taken together, the above results indicate that Leu-312 plays an important role in BK channel activation, consistent with the possibility that this S6 residue participates in interactions that directly influence the opening and closing of the gate. The effects of mutations on Ca^{2+} and voltage sensitivity, however, are surprising and suggest the influence of Leu-312 may extend beyond the gate to its interactions with Ca^{2+} and voltage sensors. To test this conclusion we analyzed the G-V data in terms of a 50-state allosteric model of BK channel gating (18), which assumes that activation of Ca^{2+} and voltage sensors independently alter the equilibrium constant L for the closed-open conformational change. Our results (Fig. 4, Table 1) support the view that Leu-312 mutations do not act merely to perturb the stability of the gate (L) but also must influence Ca^{2+}- and voltage-dependent gating processes.

The model defines the intrinsic stability of the gate by the value of L at $V = 0$ in the absence of Ca^{2+} or voltage sensor activation ($L(0)$), and the energetic coupling of sensors to the gate are described by allosteric factors (C and D) which can be defined in terms of the ratio for closed and open channels of Ca^{2+} dissociation constants ($C = K_C/K_O$) and voltage sensor equilibrium constants ($D = \exp(ZFVh_C/RT)/\exp(ZFVh_O/RT)$). Both the equilibrium constants for voltage sensor activation and channel opening are voltage-dependent and characterized by partial charges Z and Q, respectively (see "Experimental Procedures").

The WT and mutant G-V data were fit (Fig. 4, *solid lines*) by the model (Equation 2) using values of $Z = 0.58\ e$ and $Q = 0.3\ e$, determined from previous analysis of WT mSlo1 channels (19, 20). Here e is the elementary charge. In general, G-V data are not sufficient to constrain all the parameters in the allosteric model. Measurements of open probability at extreme negative voltages and/or gating currents are required, which is beyond the scope of this study and may be impossible to obtain for mutants whose activation is shifted to very negative voltages. Therefore, we did not attempt to define precisely the effect of mutation on all parameters but, rather, sought to address the simpler question, Are changes in Ca^{2+}- and voltage-dependent parameters required to account for the effects of mutation?

In the case of voltage-dependent gating the answer is clearly yes, based on the effect of mutation on G-V slope in 0 Ca^{2+}. The model predicts that large changes in the stability of the gate (L) will cause a shift of the G-V relation to more negative voltages with little change in shape, as evidenced by the predicted effect of Ca^{2+} on the WT (Fig. 4*A*). Thus, the observation that G-V relations for L312I and L312W in 0 Ca^{2+} are much shallower than the WT in 4 μM Ca^{2+} despite equivalent values of V_{50} (Figs. 1 and 2*A*) implies that the effect of mutation is not simply to change L, like Ca^{2+}. The G-V relations for L312I and L312W in 0 Ca^{2+} can be well fit by altering L to destabilize the closed relative to the open state and reducing the energetic coupling between voltage-sensor and the gate (D) (Fig. 4, *C* and *D*). In the case of L312W, a decrease in Vh_C was also required (Table 1). However, several voltage-gating parameters (D, Vh_C, Z) can affect the G-V slope in 0 Ca^{2+} (Ma *et al.* (20)), and the data are not sufficient to distinguish which combination of these parameters is altered.

As noted above, the ability of L312I to reduce both G-V slope and Ca^{2+}-dependent shifts in V_{50} requires a decreased Ca^{2+} efficacy. Consistent with this conclusion, fits to the G-V data for

FIGURE 1. **The effects of Leu-312 mutations on steady-state activation.** In *A–H*, the G-V curves shown on the *left* were generated with $[Ca^{2+}]_i$ ranging from 0 to 2 mM for mSlo1 and the mutants of Leu-312 as indicated. Representative current traces for the corresponding mutant are shown on the *right*. Currents of mSlo1 and the Leu-312 mutants were elicited from inside-out patches by voltage steps ranging from −180 to 180 mV with 20-mV increments from a holding potential of −180 mV with the cytosolic $[Ca^{2+}]_i$ as indicated. $[Ca^{2+}]_i$ are: *circle*, 0; *circle with cross-hair*, 1 μM; *square*, 4 μM; *square with cross-hair*, 10 μM; *triangle*, 300 μM; *triangle with cross-hair*, 2 mM. *Solid lines* are fits of Equation 1 (see "Experimental Procedures"). The ranges of slope factor κ are in mV/e-fold: 14.1–20.2 for mSlo1, 11.7–17.7 for L312F, 21.7–72.6 for L312I, 22.8–51.3 for L312W, 56.3–58.8 for L312C, 52.4–61.5 for L312V, 51.3–64.4 for L312S, and 53.2–68.0 for L312Q. The voltage protocol is shown at the *top*.

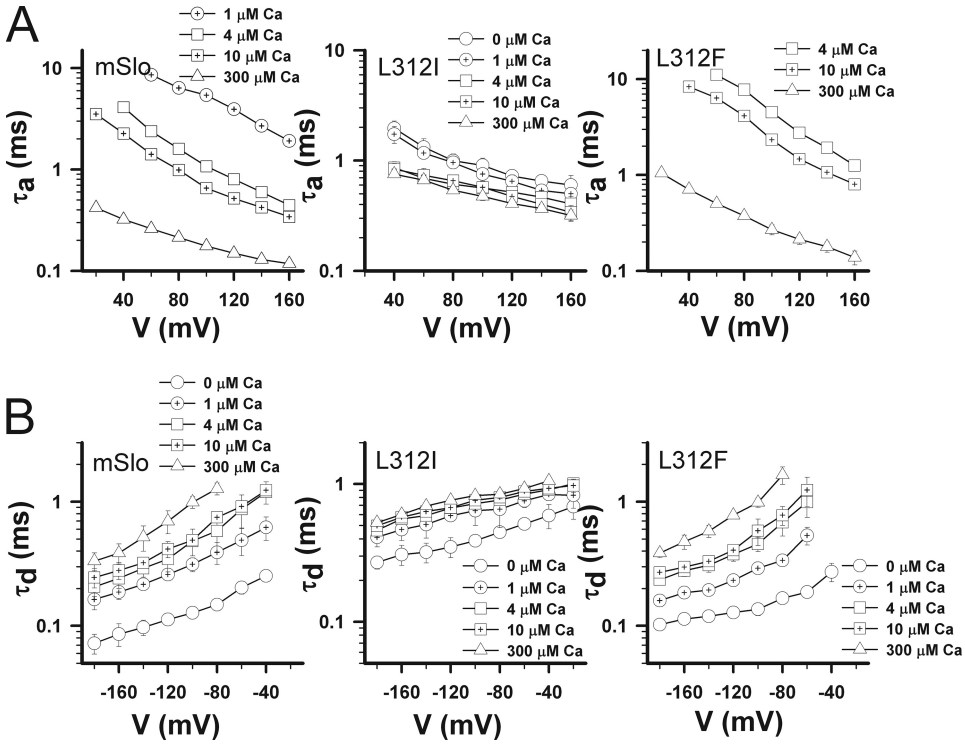

FIGURE 3. **The effects of Leu-312 mutations on activation and deactivation kinetics.** The time constants of activation (τ_a) (*A*) and deactivation (τ_d) (*B*) of currents for mSlo1, L312I, and L312F are plotted as a function of voltages in different $[Ca^{2+}]_i$. $[Ca^{2+}]_i$ are: *circle*, 0; *circle with cross-hair*,1 μM; *square*, 4 μM; *square with cross-hair*, 10 μM; *triangle*, 300 μM.

both L312I and L312W in different Ca^{2+} concentrations (Fig. 4, *C* and *D*) indicate a reduction in allosteric coupling between Ca^{2+} sensors and the gate (*C*) with little change in the open channel dissociation constant for Ca^{2+} (K_O) (Table 1). The G-Vs of the Ca^{2+}-insensitive mutants (L312C, L312S, L312V, L312Q) can be fit (*e.g.* L312Q, Fig. 4*E*) by further changes in C and L (Fig. 4, *F–H*, Table 1), consistent with the effects of L312I and L312W. The reduction of C toward unity for these mutants means that their K_C and K_O values cannot be constrained and vary widely (Table 1). However, based on the effects of L312I and L312W, we assume the Ca^{2+} insensitivity is best described as a loss of coupling ($C \approx 1$) rather than a loss of binding affinity.

Interaction of Leu-312 with Phe-315—The hypothesis that Leu-312 participates in an interaction that stabilizes the closed channel is supported by the observation that channel activation is very sensitive even to conservative mutations such as L312I, whereas more extreme substitutions (L312V, L312Q, L312S, L312C) have similar maximal effects, as if an interaction had been disrupted. Based on the structural homology shown in supplemental Fig. 1, we infer that Leu-312 probably interacts with Phe-315 in an adjacent subunit. If the effects of Leu-312 mutation on gating reflect primarily this interaction, then mutations of Phe-315 that disrupt the interaction may have a similar effect. Our results support this hypothesis but also suggest that Phe-315 plays a more critical structural role than Leu-312.

A conservative mutation of Phe-315 (F315Y) has been previously reported to greatly enhance BK channel activation without eliminating Ca^{2+} sensitivity (21, 22), qualitatively similar to L312W or L312I. However, unlike Leu-312 mutations, many Phe-315 mutations (F315A, F315G, F315I, F315L, F315T) do not give rise to measurable currents under physiological conditions (*e.g.* F315I (21)). To determine why this is the case, we examined both the current and surface expression of Myc-tagged WT and F315A mutant channels (see "Experimental Procedures"). Surprisingly, F315A was expressed in the plasma membrane at a level equivalent to the WT ($F_{F315A}/F_{WT} = 1.03$, $n = 5$), although it expressed no detectable macroscopic current in excised patches (Fig. 5*A1*), unlike the WT (Fig. 1*A*). Only brief single channel openings were observed for F315A at 200 mV (Fig. 5*A2*). Thus, we infer that the function rather than the expression of F315A is impaired.

Fortunately, we discovered one non-conservative mutant of Phe-315 (F315Q) that expressed macroscopic currents (Fig. 5*B1*) and exhibits gating properties similar to non-conservative Ca^{2+}-insensitive Leu-312 mutants. F315Q currents appear leak-like but could be completely blocked by intracellular application of 100 mM TEA (Fig. 5, *B2* and *C1*). G-V relations, determined from tail currents (Fig. 5*B2*) were shallow and shifted to very negative voltages. V_{50} in the presence and absence of $[Ca^{2+}]_i$ ranged from −144 to −196 mV, exhibiting little if any Ca^{2+} sensitivity. Thus, the effects of F315Q on gating appear similar to those of L312Q, consistent with the notion that these mutations disrupt an important interaction between Leu-312 and Phe-315.

Interestingly, G-V curves calculated from steady-state F315Q currents (Fig. 5*B3*), unlike tail currents (Fig. 5*B2*), exhibit a biphasic (double-Boltzmann) voltage dependence suggestive of voltage-dependent rectification or block in single channel conductance. Consistent with this possibility, single channel F315Q currents were extremely flickery (Fig. 5, *C1* and *C2*), in marked contrast to F315Y, which exhibits distinct open and closed events (Lippiat *et al.* (21) and Wang and Brenner (22)). The flickering single channel behavior prevented detailed analysis. However, an alteration in the permeation properties of the channel by F315Q would not be surprising given the effects of other Phe-315 mutations on single channel conductance (21).

To test for coupling of Leu-312 and Phe-315, we also constructed a double mutant L312Q/F315Q. If these residues do not interact, the ΔV_{50} of the double mutation should be approximately the sum of ΔV_{50} of L312Q and F315Q (23, 24). Unfortunately, L312Q/F315Q did not express well based on immunofluorescence and patch clamp experiments (data not shown). In any case, determining whether two residues interact directly by double-mutant cycle analysis can be problematic when the

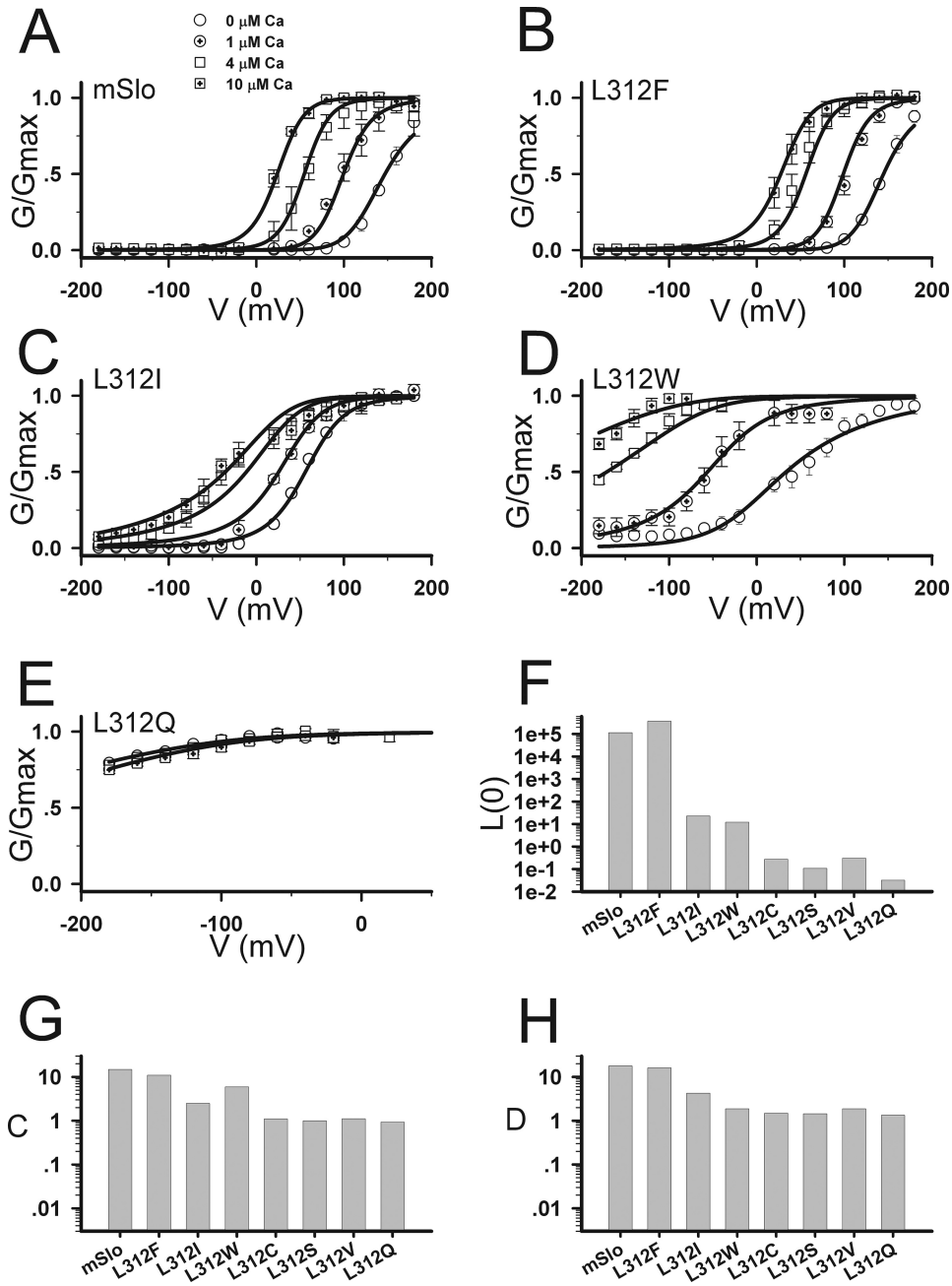

FIGURE 4. **The G-V curves of mSlo1 with the Leu-312 mutations fitted by a 50-state allosteric model.** *A–E*, G-V curves in 0–10 μM $[Ca^{2+}]_i$ for mSlo1, L312F, L312I, L312W, and L312Q as indicated were fit (*solid lines*) to Equation 2 (see "Experimental Procedures"). $[Ca^{2+}]_i$ are: *circle*, 0; *circle with cross-hair*,1 μM; *square*, 4 μM; *square with cross-hair*, 10 μM. *F–H*, the values of *L*(0); *C* and *D* are plotted for mSlo1 and mutants.

effects of individual mutations are as large as L312Q and F315Q. Therefore, we also tested for coupling of Leu-312 and Phe-315 by swapping the side chains at these positions. Consistent with the hypothesis that interaction between Leu-312 and Phe-315 holds channels closed, the double mutation L312F/F315L did not facilitate opening. Indeed the G-V curves (supplemental Fig. 4) were shifted to more positive voltages than the WT (V_{50} = 184 ± 4 mV, V_{50} = 165 ± 2 mV, V_{50} = 98 ± 1 mV, V_{50} = 56 ± 4 mV in the presence of 4, 10, 300, and 2000 μM Ca^{2+}), suggesting that the interaction is strengthened. Swapping residues is not necessarily expected to maintain a constant interaction because geometric constraints are also important. An observation supporting that the effect of L312F/F315L reflects interaction between these positions is that F315L, like most single mutations of F315, failed to express functional channels. Thus, the L312F mutation appears to partially rescue the function or expression of F315L despite the fact that L312F by itself has little or no effect on steady-state activation (Figs. 1, *A* and *B*, and 2).

Molecular Dynamics Simulation of Leu-312/Phe-315 Interaction (L-F Coupling)—To further examine whether Leu-312 interacted with Phe-315 directly, we turned to molecular dynamics simulation. Starting from an initial conformation of mSlo1 at the closed state, derived from the crystal structure of KcsA channel, we found that two residues of mSlo1, *i.e.* Leu-312 and Phe-315, could constitute a tight

TABLE 1
Summary on kinetics parameters of the 50-state allosteric model

	K_C	K_O	C	Z^a	Q^a	Vh_C	Vh_O	D	$L(0)$
	μM	μM				mV	mV		
L312F	9.450	0.858	11.014			139.434	18.086	16.150	3.717×10^5
WT	15.600	1.050	14.851	0.58*e*	0.30*e*	119.717	−5.700	17.729	1.142×10^5
L312I	3.111	1.251	2.487			101.670	38.479	4.257	22.576
L312W	5.869	0.984	5.964			−22.771	−50.242	1.877	12.061
L312C	1.002×10^{-3}	9.131×10^{-4}	1.097			−30.162	−47.499	1.488	0.272
L312S	0.948	0.954	0.994			−34.797	−50.819	1.444	0.107
L312V	2.110	1.903	1.108			−4.912	−32.329	1.875	0.306
L312Q	1.596×10^{-3}	1.707×10^{-3}	0.935			−69.896	−82.458	1.334	0.032

[a] Values are the same as in WT.

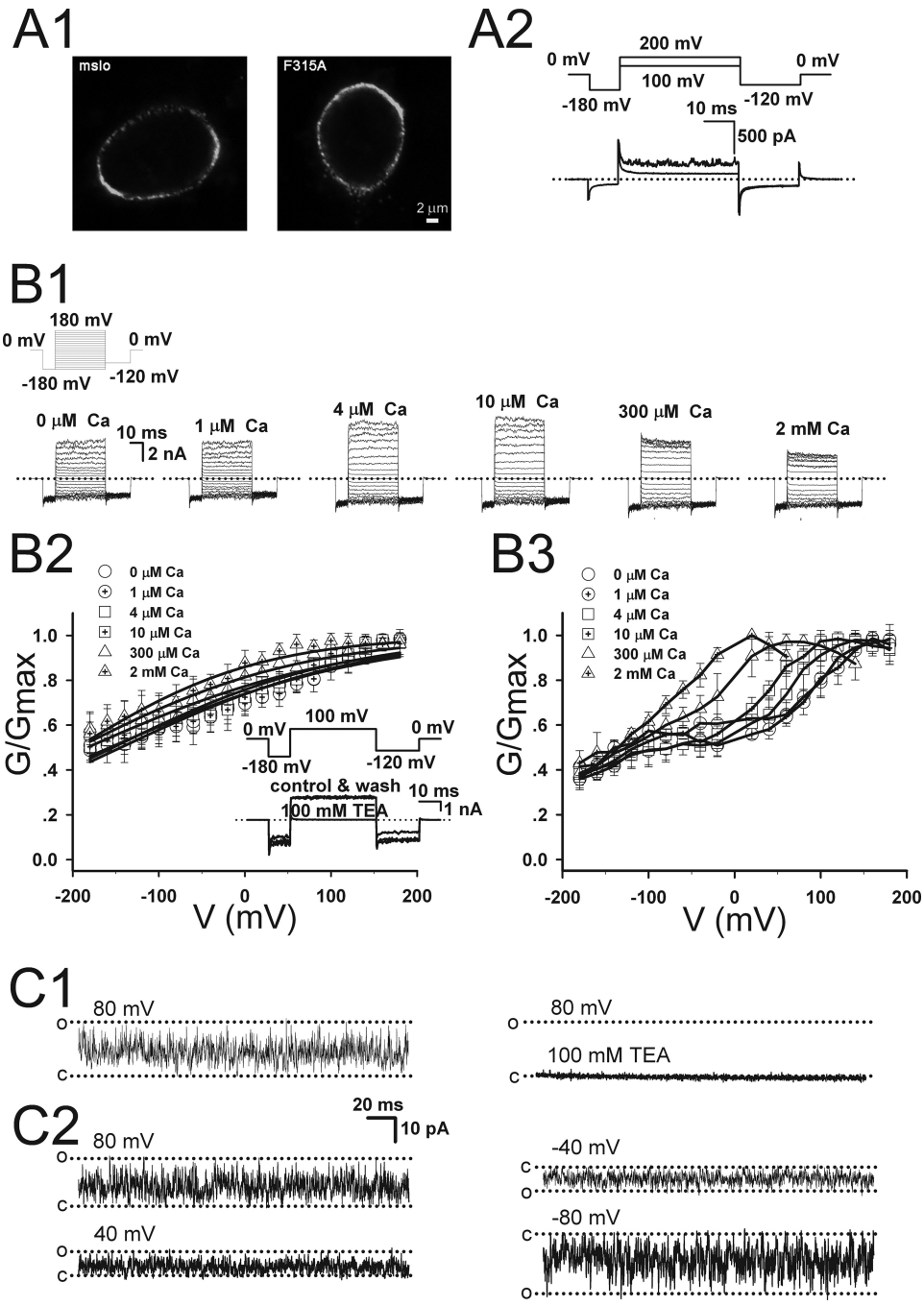

FIGURE 5. **The surface expression and the current properties of Phe-315 mutations.** *A1*, the immunofluorescence images of HEK293 cells transfected with WT mSlo1 or F315A are compared. Channels were tagged with c-Myc epitope and labeled with anti-c-Myc antibody. *A2*, the current traces of F315A channels were obtained from an inside-out patch in the presence of 10 μM Ca^{2+}. The voltage protocol is placed at the *top*. *B1*, representative current traces were obtained from inside-out patches for F315Q at different $[Ca^{2+}]_i$. Voltage steps placed at the top were executed from −180 to 180 mV by 20-mV increments after 20 ms at −180 mV and then returned to −120 mV. The G-V curves were generated over $[Ca^{2+}]_i$ from 0 to 2 mM for F315Q by tail currents (*B2*) and steady-state currents (*B3*). The intracellular $[Ca^{2+}]_i$ are: *circle*, 0; *circle with cross-hair*, 1 μM; *square*, 4 μM; *square with cross-hair*, 10 μM; *triangle*, 300 μM; *triangle with cross-hair*, 2 mM. The *inset* shows representative current traces from inside-out patches in 10 μM $[Ca^{2+}]_i$, which were elicited in before (control), during, and after (wash) application of 100 mM TEA. The voltage protocol is placed at the *top* of the *inset*. The *dotted lines* represent zero current. *C1*, single-channel currents of F315Q were obtained at 80 mV in the presence of 10 μM Ca^{2+} with/without 100 mM TEA as indicated. *C2*, the single-channel currents of F315Q were obtained at 80, 40, −40, and −80 mV in the presence of 10 μM Ca^{2+}.

structure when an equilibrated conformation was achieved (Fig. 6*A1*) compared with loose (Fig. 6*B1*) and tight (Fig. 6*C1*) structures of L312I and L312F, respectively. The side chain of Leu-312 with a symmetrical Y-apex was tightly "locked" within a distance of ~3 Å by the aromatic ring of Phe-315 in the adjacent subunit (Fig. 6*A1*). Additionally, the mean distance between Leu-312 and Phe-315 was mostly maintained constant all the time because of strong interaction (Fig. 6*A2*). Similarly, the side chain of Phe-312 with an aromatic ring was more tightly locked, because of the markedly overlapped area, within a distance of ~3.0 Å by the aromatic ring of Phe-315 in the adjacent subunit (Fig. 6, *C1–C3*). In contrast, the side chain of Ile-312 with an asymmetrical Y-apex was less tightly locked within a distance of ~3.6 Å by the aromatic ring of Phe-315 in the adjacent subunit (Fig. 6*B1*). With randomly swinging of each side chains, the asymmetrical side chain of Ile-312 may gradually deviate from the aromatic ring of Phe-315 as time elapses (Fig. 6, *B2–B3*). Therefore, symmetry of the side chain of leucine may produce a maximal effect on the aromatic ring of phenylalanine, named L-F coupling. Such intimate interaction reveals that a L-F coupling, existing in the closed structural conformation of BK channels, locks the channel to the closed state.

The Single-channel Properties of Ca^{2+}-insensitive Leu-312 Mutants—The macroscopic G-V relations for L312C, L312V, L312S, L312Q (Fig. 1, *E–H*) indicate that these channels are maximally activated even at very negative voltages. To confirm that maximal activation represents an open probability (P_O) near unity, as in the WT, and to better understand the lack of Ca^{2+} sensitivity, we examined the single channel properties of L312S (Fig. 7). The P_O of L312S was almost 100% at 80, 40, −40, and −80 mV in the absence of Ca^{2+} (Fig. 7*A*) and is similar for L312Q (supplemental Fig. 5), indicating that the mutants are almost permanently open under physiological conditions. Correspondingly, the amplitude histogram of L312S contains a large open component and a tiny closed component at all voltages (Fig. 7*A*). The kinetics of single WT BK channels are typically complex, even in the absence of Ca^{2+}-containing multiple closed and open components,

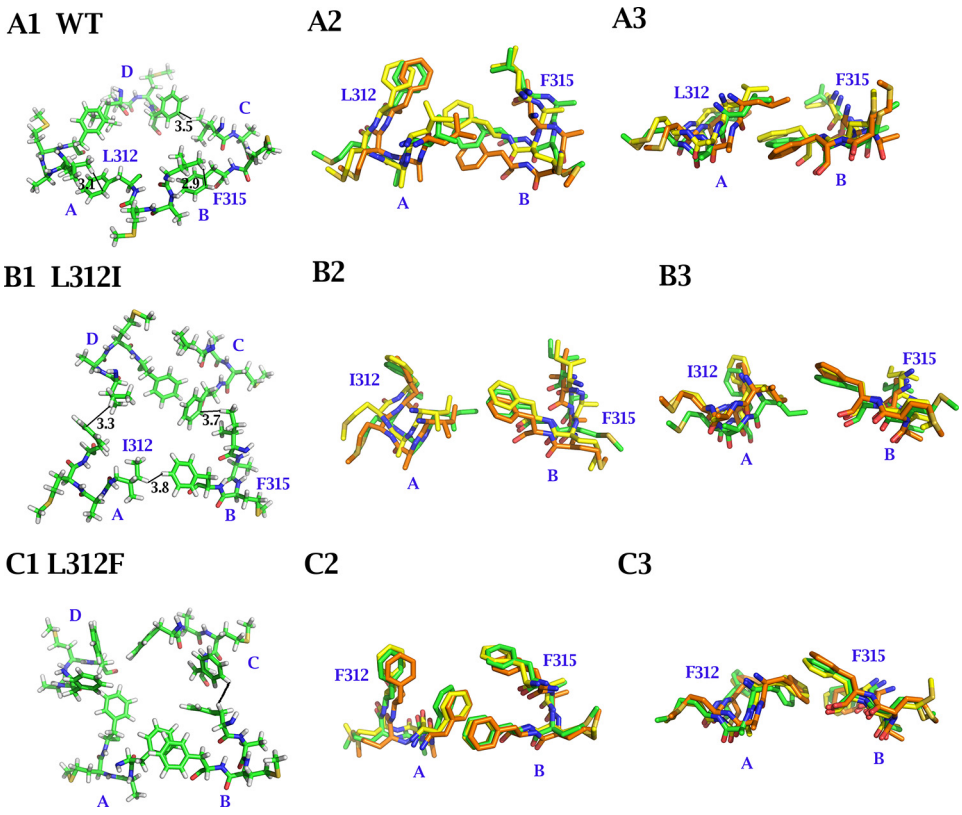

FIGURE 6. **Comparison between the pore structures of WT mSlo1, L312I, and L312F in the closed conformation.** *A*, *B*, and *C*, truncated closed pore structures of WT, L312I, and L312F, respectively, were derived from homologous modeling using KcsA (PDB code 1BL8) as a template followed by 2-ns molecular dynamic simulations In *A1*, *B1*, and *C1*, equilibrated structures of the residue at position 312 together with Phe-315 are viewed from the top in all four subunits. In *A2*, *B2*, and *C2*, for clarity, only one interacting pattern between Leu-312 and Phe-315 of mSlo1 is viewed from the top. In *A3*, *B3*, and *C3*, the same interacting pattern between Leu-312 and Phe-315 of mSlo1 is viewed laterally. Each pair of structures colored in *green*, *yellow*, and *brown* represents different interacting patterns between Leu-312 and Phe-315, which were acquired at different times during the 2-ns simulation. The mean distances between Leu-312/Phe-315, Ile-312/Phe-315, or Phe-312/Phe-315 in the closed conformation are 3.08 ± 0.31 Å ($n = 4$), 3.68 ± 0.26 Å ($n = 4$), or 3.02 ± 0.28 Å ($n = 4$), respectively.

reflecting that channels contain multiple voltage sensors that may be activated (25). By contrast, the dwell-time distribution histograms of L312S (Fig. 7*A*) appear to be characterized by a single open and closed component. We fit the data with a simplified model containing two open and two closed states (2C-2O) (13) but found that the kinetics of L312S were effectively described by a single open and closed time constant, because two open time constants predicted by the model were almost equal, and the weight (or fraction) of the slow closed time constant was small (Fig. 7*B*). Although it is possible that we failed to resolve multiple closed components because the mean closed time was brief (~1 ms), the apparent two-state kinetics suggest that the opening and closing of L312S in 0 Ca^{2+} reflects a concerted process. Such behavior could arise, for example, if the mutation caused voltage sensors to be constitutively activated (decreasing Vh_C in the allosteric model) or decoupled from the gate ($D \approx 1$) so that the opening and closing of a pore gate (*i.e.* the inner helix) is unaffected by the voltage sensors.

Even though there were distinct differences between WT and calcium-insensitive mutants in their P_O and kinetics, the single-channel conductance of L312S, L312Q, and L312V were indistinguishable from the WT (~250 picosiemens) in 160 mM K^+ symmetrical solutions (Fig. 7*C*). That these mutants have no effect on single channel conductance of BK channels is consistent with the notion that they promote channel opening without altering the open conformation of the pore.

DISCUSSION

With the help of several techniques such as electrophysiology, mutagenesis, and immunofluorescence, we demonstrate that an L-F coupling structure can keep the pore of BK channel in the closed state. Once their connection was disrupted completely, channels open permanently under physiological conditions without changing single-channel conductance, suggesting that this coupling plays a critical role in the pore of BK channel. However, it is still difficult to interpret all the phenomena observed in this study.

Is Amino Acid Bulk or Hydropathy Alone Sufficient to Explain the Effects of Leu-312 Mutations?—We observed an increased effect of Leu-312 mutation on gating with hydrophilic and/or small side-chain substitutions. We attempted to understand these effects in terms of the physical properties of substituted amino acids. For example, some mutations of Leu-312 (Gln, Ser, Cys, Val) eliminated calcium sensitivity, whereas others (Phe, Ile, Leu, Trp) maintained it. The hydrophobicity of glutamine, serine, valine, and cysteine spans the Sweet-Eisenberg hydropathy range from a hydrophobic 0.91 (Val) to a hydrophilic −0.91 (Gln) (26). Phenylalanine, leucine, and isoleucine have positive hydropathy indexes 1.92, 1.22, and 1.25, respectively, and each retained calcium sensitivity to some degree. Tryptophan also retained calcium sensitivity but has a positive hydropathy index 0.5 smaller than that of valine. These observations suggest that hydropathy cannot completely explain the effects of the mutations at position Leu-312. By contrast, there is a clear demarcation between Ca sensitivity and apparent molecular volumes (27). All of the amino acid substitutions, which eliminated calcium sensitivity, were less than 166.7 $Å^3$, the volume of leucine. All the mutations (Trp, Ile, and Phe), which retained calcium sensitivity, were equal to or larger than leucine. These results suggest that the bulk of the side chain at position Leu-312 may exert some effects on Ca^{2+}-dependent gating.

By contrast, the shifts in the G-V relationships by mutation are not easily related to either the hydrophobicity or volume of the substituted amino acid. This point is illustrated in Fig. 8 by plotting the V_{50} of each mutant as a function of $[Ca^{2+}]_i$ together with the volume (Fig. 8*A*) or hydrophobicity (Fig. 8*B*) of the

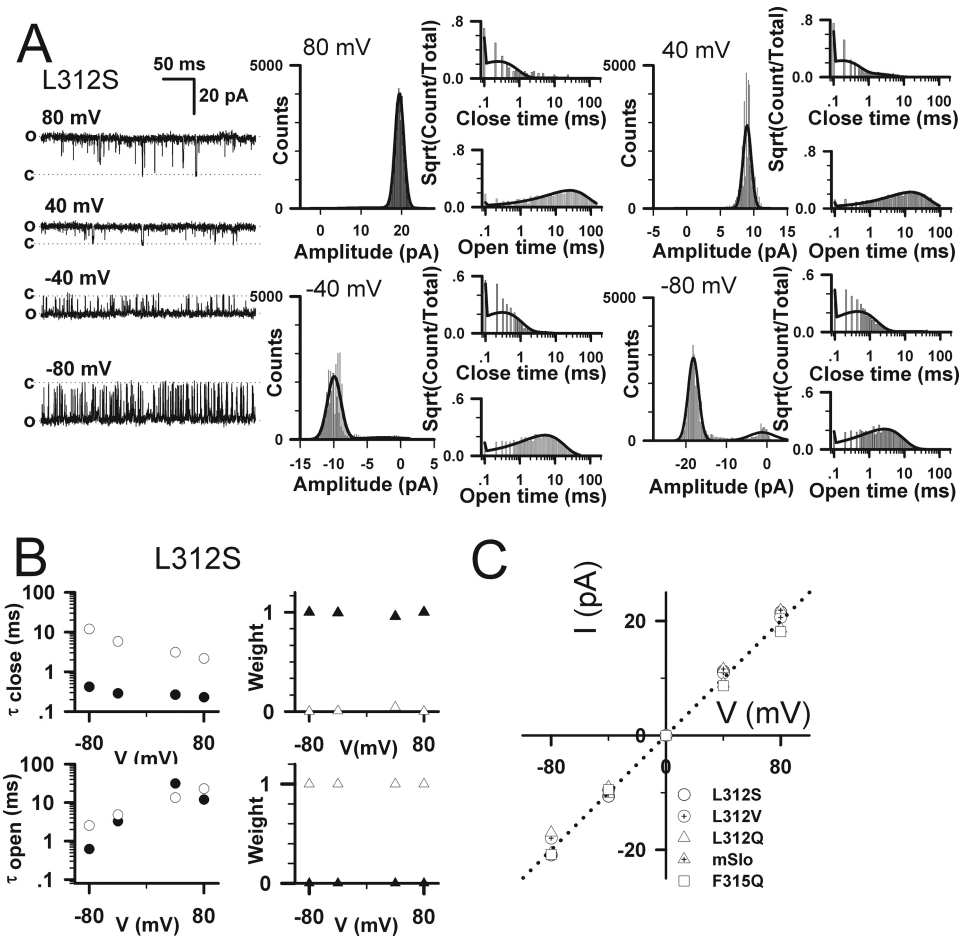

FIGURE 7. **Kinetics and conductance of single-channel L312S currents.** The single-channel currents of L312S (*A*) were obtained from inside-out patches at voltages as indicated in the presence of 0 $[Ca^{2+}]_i$. All the single-channel currents were filtered at 10 kHz. The *dashed line* labeled with a letter *c* or *o* represents the closed or open level, respectively. Amplitude histograms of currents and dwell-time distributions are shown for L312S (*A*). Both the open and closed time constants were best fitted to a biexponential function with the software QuB. Time constants with their relative weights are plotted for L312S (*B*). The *open circles* are for the slow closed/open time constants, the *filled circles* are for the fast closed/open time constants, the *open triangles* are for the weight of the slow closed/open time constants, and the *filled triangles* are for the weight of the fast closed/open time constants. *C*, the single-channel current-voltage (I-V) curves are plotted for mSlo1 alone, L312S, L312Q, L312V, and F315Q as indicated. Levels of single-channel currents were measured by eye.

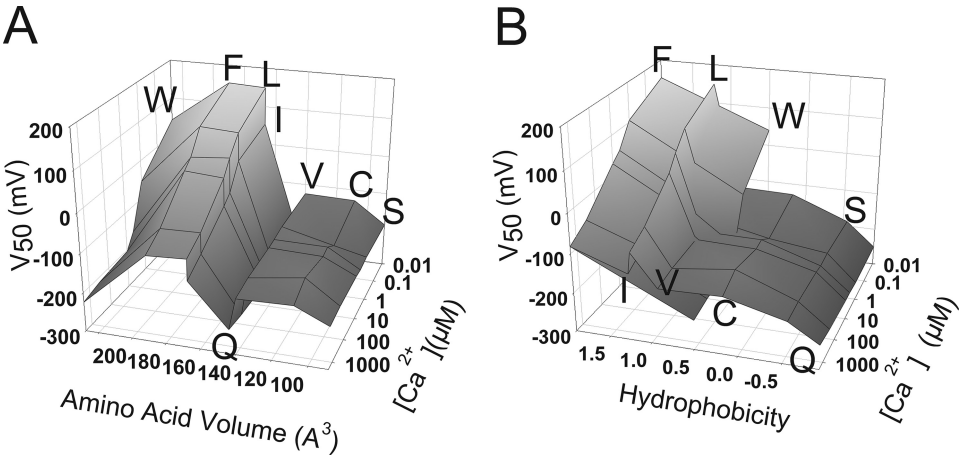

FIGURE 8. **The effects of volume and hydrophobicity on V_{50}.** The three-dimensional plots among V_{50}, $[Ca^{2+}]_i$, and volume (*A*) or hydrophobicity (*B*) are plotted for each mutant. The values of volume (Å^3)/hydrophobicity (arbitrary units) are: 89/−0.55 for serine, 108.5/0.17 for cysteine, 140/0.91 for valine, 143.8/−0.91 for glutamine, 166.7/1.25 for isoleucine, 166.7/1.22 for leucine, 189.9/1.92 for phenylalanine, and 227.8/0.5 for tryptophan (26, 27).

substituted amino acid (26, 27). Again, V_{50} goes up and down with increased hydrophobicity or volume of the substituted amino acid, suggesting that neither parameter alone can account for the G-V shift. Indeed, the GV curves of L312I are shifted by −50 to −80 mV relative to the WT at all the Ca^{2+} concentrations even though Leu and Ile have the same hydropathy index and volume. Therefore, we conclude that the specific structural conformation, as in L-F coupling, is also critical to channel gating.

How Can Intersubunit Coupling Structure Keep the BK Channel Pore Closed?—Among the Leu-312 mutations, only L312F can also maintain the G-V curves similar to that of WT mSlo1 probably because of the strong π-π interaction between two aromatic rings. Although isoleucine lacks one methyl at the end of its side chain compared with leucine side chain, its hydrophobicity is similar to that of leucine. However, such a tiny difference makes Ile-312 unable to form a tight interaction with Phe-315 and leads to significant changes in gating. Just because of limitations in the length, symmetry, and hydrophobicity of side chains, Leu-312 mutations such as cysteine, glutamine, serine, and valine residues could seriously disrupt the intersubunit coupling structure and lead to an ostensible "leak" current. In addition, the aromatic ring of the amino acid Phe-315 is equally essential to keep the regular structure and function of BK channels. Such importance was demonstrated by the glutamine substitution F315Q, which also led to a "permanently-open," Ca^{2+}-insensitive channel. Therefore, the L-F structure of mSlo1 provides a model for us to gain an insight into the intersubunit coupling function in BK-type channels.

How Do Leu-312 Mutations Eliminate Ca^{2+} Sensitivity?—In terms of the allosteric model of BK channel gating, it is impossible to account for a complete lack of Ca^{2+} sensitivity, as observed for L312C, L312V, L312S, L312Q, without reducing

the allosteric factor C to unity or increasing the Ca^{2+} dissociation constants (K_C, K_O) far above the experimental range (2 mM). Thus, these mutations may disrupt interactions between Ca^{2+} sensors and the gate. Likewise, a decoupling of voltage sensors from the gating could cause the apparent two-state behavior in single-channel kinetics of L312S. However, an interesting alternative possibility is that, by disrupting interaction of Leu-312 with Phe-315, mutations such as L312S cause the pore gate to be permanently opened, and the residual flickering closings observed at negative voltages represent a property of the selectivity filter. In this way the channel could become Ca^{2+}-insensitive without requiring that Ca^{2+} sensors become decoupled from the pore gate. Rather, the influence of Ca^{2+} and voltage sensors may be reduced because the open probability of the pore gate is saturated.

Acknowledgment—We thank Dr. Charles Bowman for valuable suggestions.

REFERENCES

1. McManus, O. B. (1991) *J. Bioenerg. Biomembr.* **23,** 537–560
2. Atkinson, N. S., Robertson, G. A., and Ganetzky, B. (1991) *Science* **253,** 551–555
3. Adelman, J. P., Shen, K. Z., Kavanaugh, M. P., Warren, R. A., Wu, Y. N., Lagrutta, A., Bond, C. T., and North, R. A. (1992) *Neuron* **9,** 209–216
4. Butler, A., Tsunoda, S., McCobb, D. P., Wei, A., and Salkoff, L. (1993) *Science* **261,** 221–224
5. Salkoff, L., Butler, A., Ferreira, G., Santi, C., and Wei, A. (2006) *Nat. Rev. Neurosci.* **7,** 921–931
6. Hille, B. (2001) *Ionic Channels of Excitable Membranes*, 3rd Ed., Sinauer Associates Inc., Sunderland, Massachusetts
7. Brelidze, T. I., Niu, X., and Magleby, K. L. (2003) *Proc. Natl. Acad. Sci. U.S.A.* **100,** 9017–9022
8. Li, W., and Aldrich, R. W. (2004) *J. Gen. Physiol.* **124,** 43–57
9. Liu, Y., Holmgren, M., Jurman, M. E., and Yellen, G. (1997) *Neuron* **19,** 175–184
10. Magidovich, E., and Yifrach, O. (2004) *Biochemistry* **43,** 13242–13247
11. Webster, S. M., Del Camino, D., Dekker, J. P., and Yellen, G. (2004) *Nature* **428,** 864–868
12. Doyle, D. A., Morais Cabral, J., Pfuetzner, R. A., Kuo, A., Gulbis, J. M., Cohen, S. L., Chait, B. T., and MacKinnon, R. (1998) *Science* **280,** 69–77
13. Guo, Z., Lv, C., Yi, H., Xiong, Y., Wu, Y., Li, W., Xu, T., and Ding, J. (2008) *Biophys. J.* **94,** 3714–3725
14. Li, H., Yao, J., Tong, X., Guo, Z., Wu, Y., Sun, L., Pan, N., Wu, H., Xu, T., and Ding, J. (2007) *J. Biol. Chem.* **282,** 17720–17728
15. Case, D. A., Darden, T. A., Cheatham, T. E., Simmerling, C. L., Wang, J., Duke, R. E., Luo, R., Merz, K. M., Wang, B., Pearlman, D. A., Crowley, M., Brozell, S., Tsui, V., Gohlke, H., Mongan, J., Hornak, V., Cui, G., Beroza, P., Schafmeister, C., Caldwell, J. W., Ross, W. S., and Kollman, P. A. (2004) *Amber 8*, University of California Press, San Francisco
16. Long, S. B., Campbell, E. B., and Mackinnon, R. (2005) *Science* **309,** 897–903
17. Cui, J., and Aldrich, R. W. (2000) *Biochemistry* **39,** 15612–15619
18. Cox, D. H., and Aldrich, R. W. (2000) *J. Gen. Physiol.* **116,** 411–432
19. Horrigan, F. T., and Aldrich, R. W. (2002) *J. Gen. Physiol.* **120,** 267–305
20. Ma, Z., Lou, X. J., and Horrigan, F. T. (2006) *J. Gen. Physiol.* **127,** 309–328
21. Lippiat, J. D., Standen, N. B., and Davies, N. W. (2000) *J. Physiol.* **529,** 131–138
22. Wang, B., and Brenner, R. (2006) *J. Gen. Physiol.* **128,** 731–744
23. Carter, P. J., Winter, G., Wilkinson, A. J., and Fersht, A. R. (1984) *Cell* **38,** 835–840
24. Sadovsky, E., and Yifrach, O. (2007) *Proc. Natl. Acad. Sci. U.S.A.* **104,** 19813–19818
25. Talukder, G., and Aldrich, R. W. (2000) *Biophys. J.* **78,** 761–772
26. Ellington, A., and Cherry, J. M. (2001) *Curr. Protoc. Mol. Biol.* Appendix 1, Appendix 1C
27. Zamyatnin, A. A. (1972) *Prog. Biophys. Mol. Biol.* **24,** 107–123